Multi-dimensional time-correlated single photon counting applied to diffuse optical tomography

Wolfgang Becker[1], Axel Bergmann[1], Adam Gibson[2], Nick Everdell[2], David Jennions[2], M. Schweiger[3], S. R. Arridge[3], Jeremy C. Hebden[2]
[1]Becker & Hickl GmbH, Nahmitzer Damm 30, 12277 Berlin, Germany
[2]Department of Medical Physics & Bioengineering, University College London, UK
[3]Department of Computer Science, University College London, UK

Abstract

We present a multi-dimensional TCSPC technique that combines multi-detector and multiplexing capability, and records fast and virtually unlimited sequences of time-of-flight distributions. The system consists of four fully parallel TCSPC channels. Each channel records simultaneously in up to eight detection channels. Up to four lasers and 32 source positions can be multiplexed. The total count rate is up to 4×10^7 photons per second. Time-of-flight sequences can be recorded with a resolution of 50 to 100 ms per curve. The system is operated within a single personal computer.

Keywords: TCSPC, Diffuse Optical Tomography, Brain Imaging.

1. INTRODUCTION

The technique known as diffuse optical tomography (DOT) is being developed to image the spatial distribution of optical properties within highly scattering media. Biomedical applications of DOT generally involve illuminating thick regions of tissue with near-infrared (NIR) light and detecting the diffusely transmitted or reflected light, or the fluorescence of endogenous or exogenous fluorophores [23,43]. Typical applications of DOT techniques are optical mammography, brain imaging, and non-invasive investigations of drug effects in small animals. Despite its relatively poor spatial resolution, DOT has the benefit that the measured absorption coefficients are related to the biochemical constitution of the tissue, such as haemoglobin concentration and blood oxygenation [12, 28]. If exogenous markers are used the absorption or fluorescence delivers additional information about blood flow, blood leakage, ion concentrations, or the binding state to proteins [13,24,31, 39].

The effects of scattering, absorption, and fluorescence are difficult to distinguish in steady state images of the diffusely transmitted or reflected intensity. The distinction is much easier for pulsed or modulated illumination and time-resolved detection. The shape of the time-of-flight distribution of the photons can then be used to separate between scattering and absorption [10,12,21,42]. Moreover, the depth of scattering and absorption changes in the tissue can be derived from time-resolved data [14,25,26,40]. The advantage of time-resolved detection is obvious if fluorescence is to be detected [11,15,17,30,37,39]. The fluorescence lifetime of a fluorophore is, to a first approximation, independent of its concentration, but depends on the local environment and the binding state [24]. Fluorescence measurements in DOT target either intensity and lifetime changes induced by differences in the local environment parameters, or the study of blood content and blood-flow dynamics by fluorophores that stay exclusively in the blood.

Clinical applications of optical tomography techniques are currently at the stage of tests on human subjects [19,22,27,41]. Frequency-domain instruments using modulation techniques [10,29,30] and time-domain instruments using time-correlated single-photon counting (TCSPC) [18,34,38,42] are both being evaluated. It is commonly believed that frequency-domain techniques achieve shorter acquisition times, whereas time-domain techniques deliver a better absolute accuracy of optical tissue properties.

A comprehensive overview of frequency domain DOT techniques is given in [10]. The benefit of the frequency-domain techniques is their short acquisition times at high detection intensities. To obtain unambiguous results, the phase and the amplitude of the signals have to be measured at a large number of modulation frequencies. Another problem is that crosstalk between the amplitude and the phase is difficult to avoid, which makes it difficult to obtain absolute optical tissue properties. A carefully designed system [33] has achieved a systematic phase error of 0.5° at 100 MHz. Another system that compensates for the amplitude-phase crosstalk via a reference channel reached an rms phase error of 0.2° at

100 MHz [32]. These phase errors correspond to a time shift of 14 ps and 5.5 ps rms, respectively. TCSPC [36] is superior in terms of efficiency and sensitivity. Moreover, the effective detection bandwidth is much higher than for frequency-domain systems. The amplitude-dependent shift of the instrument response function can be kept below 2 ps peak-to-peak, or about 1 ps rms. However, the count rate of TCSPC is limited to a few MHz per TCSPC channel, which is often considered a drawback. It should, however, be taken into account that TCSPC obtains a better signal-to-noise ratio (SNR) from a given number of detected photons than any other technique. Therefore the limited count rate is less important than commonly believed. The excellent results obtained with TCSPC-based DOT instruments under clinical conditions [18,19,22,27,41] demonstrate the applicability of TCSPC.

2. TCSPC TECHNIQUE

Time-domain DOT requires a detection system with an instrument response function (IRF) width as short as 100 ps to 200 ps. The time-channel width should be shorter than 10 ps [35]. The time-of-flight distributions have to be recorded simultaneously at a large number of detector positions [34,38]. For experiments with white light [2] and for fluorescence applications multi-spectral detection may be required. The resolution of haemodynamic effects requires fast sequential recording of a large number of time-of-flight distributions [26]. Moreover, different source positions and lasers of different wavelength must be multiplexed. For small-animal imaging, optical scanning by fast, galvanometer driven mirrors may be useful [17].

Multi-dimensional TCSPC

A suitable time-domain technique exists in form of the recently introduced multi-dimensional TCSPC technique. The technique uses a multi-dimensional recording process. Photon counts versus the time-of-flight are build up in a fluorescence decay or a time-of-flight distribution, as a function of either the time from the start of the experiment, the detector channel number or detection wavelength, several multiplexed lasers or source positions, or the spatial coordinates of a scanning area. Compared to early TCSPC setups [36], advanced TCSPC devices can be operated at count rates of more than two orders of magnitude higher [3,4].

The typical configuration of TCSPC for DOT is shown in Fig. 1. At the input of the detection system are a number of photomultipliers (PMTs), detecting signals from different positions on the sample or at different wavelength intervals. In the subsequent router the single-photon pulses of the PMTs are combined into a common timing pulse line. Furthermore, the router generates a digital 'channel' signal that represents the number of the PMT in which a photon was detected. The TCSPC module measures the times of the single-photon pulses and receives the corresponding 'channel' data words. Both variables are used as independent dimensions of the photon distribution to be built up. The routing technique can be used with several individual PMTs [3, 34] and with a multi-anode PMT [6].

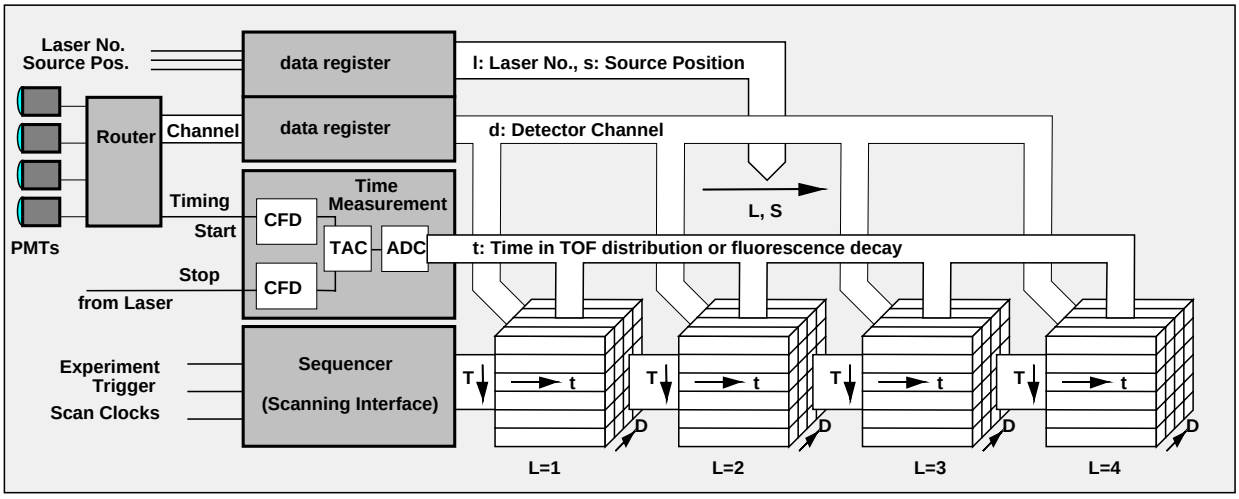

Fig. 1: Multidimensional TCSPC for DOT.

An additional data register is provided for multiplexing several lasers or source positions. Diode lasers can be multiplexed electronically at rates up to about 100 kHz [9]. In principle, fast fibre switches can be operated at rates in the 100 Hz range. The TCSPC device accepts a data word that contains the number of the currently active laser and the number of the active source channel. These numbers are used as independent coordinates of the recording process. One or two additional dimensions are added by the sequencer block of the TCSPC device. The sequencer is a programmable logical device. In DOT applications it is mainly used to record fast sequences of TOF curves. The sequencer then delivers a data word representing the time from the start of the experiment or from an external experiment-trigger pulse. In scanning applications the sequencer receives synchronisation pulses from an optical scanner and determines the location of the beam in the scanning area [5]. For each photon, the TCSPC module determines the time, *t*, of the photon in the laser pulse sequence, the detector channel number, *d*, the source position, *s*, the active laser, *l*, and the time from the start of the experiment, *T*. These values are used to address a memory in which the detected events are stored. Thus, the distributions of photon density are accumulated in the memory as a function of *t*, *d*, *s*, *l*, and *T*.

The data acquisition may run at any sequencing or multiplexing rate. It is only required that the sequencing and multiplexing is either performed at clearly different rates or is synchronised. The sequencing and multiplexing rates can even be higher than the photon count rate. This makes the recording process more or less random. As many sequencer runs and multiplexing cycles can be accumulated as necessary to obtain an appropriate SNR. It should be noted that multi-dimensional TCSPC does not use any time gating, wavelength scanning, or detector multiplexing. For count rates up to a few MHz virtually all detected photons contribute to the result. Consequently, a near-ideal SNR for a given signal intensity and acquisition time is obtained.

The time resolution is determined mainly by the transit time spread of the detectors. With microchannel-plate PMTs the width of the IRF is typically 25 ps to 30 ps (FWHM) [5]. The detectors typically used for DOT deliver an IRF width of 140 ps to 180 ps [3]. Moreover, the time-of-flight functions in the individual *d*, *T*, *s*, and *l* channels are resolved into a large number (typically 256 to 4096) time channels. Consequently, the signals are adequately sampled to satisfy the Nyquist criterion. The time-of-flight functions or multi-exponential fluorescence decay profiles are therefore unambiguously resolved.

Dual-Memory Architecture

In the configuration shown in Fig. 1 the product of the number of detector channels, **D**, the number of multiplexed lasers, **L**, and source positions, **S**, and the number of sequencer steps, **N**, is limited by the available memory space. Currently, for the largest TCSPC modules and a number of time-channels of 1024 per curve, the maximum product **D.L.S.N** is 16,384 [8]. By triggering the sequencer synchronously with the stimulation and accumulating over a large number of stimulation events very fast, reasonable long sequences can be recorded. However, in DOT it is difficult to remove the effect of the heart beat or motion artefacts from the accumulated data. Therefore it is usually preferred to record a continuous sequence of TOF data over a large number of stimulation events. Fig. 2 shows how a virtually infinite sequence of TOF data is recorded.

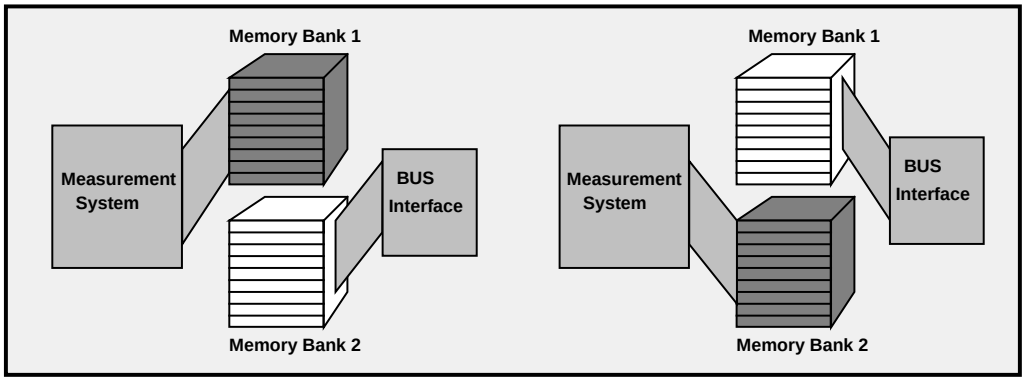

Fig. 2: Continuous recording of a TOF sequence by memory swapping.

The TCSPC device contains two identical memory banks of the structure shown in Fig. 1. While the measurement system records a sequence of photon distributions into the first memory bank the host computer reads the data of the second bank. When the first bank is filled the banks are swapped and the recording continues. As long as the readout is faster than the data acquisition a virtually unlimited, gap-free sequence of TOF data is obtained. Depending on the number of time channels, detectors, and source and laser multiplexing channels, gap-free recording can be achieved for sequencer rates as fast as 1 ms to a few 100 ms per TOF distribution. The technique was originally developed for single-molecule detection and DNA sequencing in a microcapillary flow setup [7]. It is therefore often termed "continuous flow" mode.

Pile-up effect

A single TCSPC channel is unable to record a second photon during a single signal period. Arrival (and loss) of a second photon is more likely to occur during the later part of the period, and therefore the recorded distribution is distorted. Pile-up distortion becomes noticeable if the count rate exceeds a few percent of the pulse repetition rate. Classic pile-up was the dominating source of signal distortion in early TCSPC experiments. The excitation sources of that time had repetition rates of a few 10 kHz. Therefore severe pile-up occurred at count rates higher than a few kHz. The currently used diode, titanium-sapphire, or fibre lasers have repetition rates of 50 to 80 MHz, and consequently pile-up effects are considerably reduced. The pile-up-distortion is predictable and correctable [36]. For a single-exponential fluorescence decay function the influence of the pile-up on the recorded lifetime can be explicitly calculated. The recorded lifetime, τ_{rec}, for a lifetime, τ, of the fluorescence decay and an average number of photons, P, per signal period is:

$$\tau_{rec} = \tau \frac{1 + \frac{1}{2}\frac{1}{2!}P + \frac{1}{3}\frac{1}{3!}P^2 + \frac{1}{4}\frac{1}{4!}P^3 + \ldots}{1 + \frac{1}{2!}P + \frac{1}{3!}P^2 + \frac{1}{4!}P^3 + \ldots..}, \quad \text{or} \quad \tau_{rec} \cong \tau\left(1 - P/4\right) \text{ for } P < 0.1 .$$

The maximum reasonable count rate of a TCSC channel of 100 ns dead time is about 5 MHz. For a typical lifetime of 500 ps and a laser repetition rate of 50 MHz the pile-up error is 12.5 ps. This is not more than the amplitude-phase crosstalk in good frequency-domain systems [32,33]. In multi-dimensional TCSPC the pile-up error is further reduced by the multi-detector technique. Several photons arriving during one signal period are more likely to be detected in different detector channels than in the same one. The router recognises such events and rejects both photons [8].

Multi-module technique

The pile-up effect and the degradation of the detector response limits the effective (recorded) count rate to about 5 MHz per TCSPC channel. Moreover, the dead time of the currently used TCSPC devices is of the order of 100 ns. Thus, the devices lose about 50% of the detected photons at a detector count rate of 10 MHz. Higher count rates can be achieved by operating several TCSPC channels in parallel. Four parallel channels can be operated in a single standard PC. A four-channel system for optical tomography is described in [3], and a similar system for laser scanning microscopy in [4]. Applications to DOT are described in [26,27,41,42].

3. TEST OF THE SYSTEM

Timing stability of the detectors

For count rates in the MHz range the instrument response of a TCSPC system is not necessarily independent of the count rate. Systematic timing shifts may occur as a result of count-rate-induced temperature and voltage variations in the electronic system. However, the most critical parts of the system are the PMT and its voltage divider. Changes in the count rate induce changes in the voltage distribution across the dynodes and, consequently, changes in the transit time. The IRF stability of a number of different PMTs was tested with an SPC-144 TCSPC module and a BHL-600 diode laser (both Becker & Hickl, Berlin). The pulse repetition rate was 50 MHz. The best results were obtained with the Hamamatsu H5773 photosensor modules. Fig. 3 shows eight IRF recordings for (recorded) count rates from 30 kHz to 4 MHz. The measurements were stopped when the peak of the curve reached 65,535 counts. Neither in the linear plot

(left) nor in the logarithmic plot (right) is any change in the IRF shape apparent. The first moments of all recordings are identical within 2 ps. The surprisingly high timing stability may in part be a result of the Cockroft-Walton voltage-divider design of the H5773 modules [20].

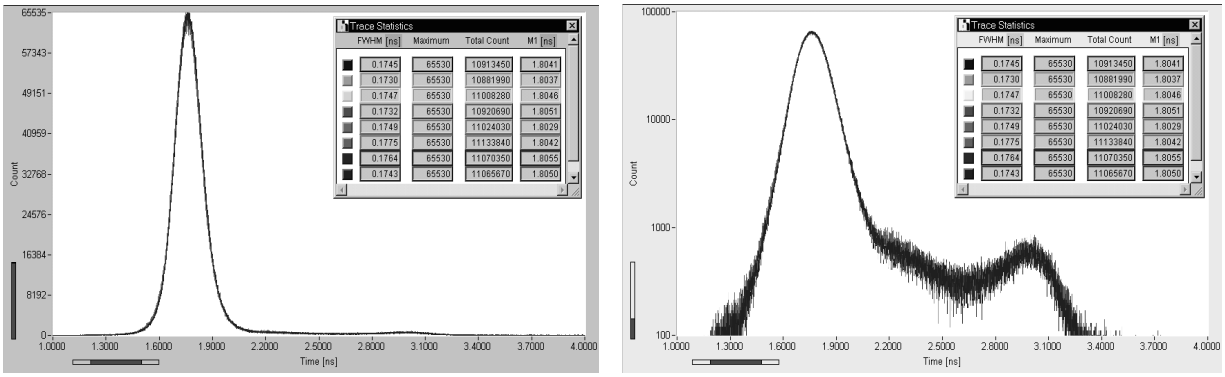

Fig. 3: IRF of an H5773-20 photosensor module for different count rates ranging from 30 kHz to 4 MHz. Linear scale (left) and logarithmic scale (right). The shift of the IRF is <2 ps and not discernible in the curves.

Signal quality

Fig. 4 shows 20 time-of-flight curves selected from a longer sequence. The curves were recorded using a single H5773-20 detector connected to one channel of an SPC-134 four-channel TCSPC package (Becker & Hickl, Berlin). The acquisition time was 100 ms per curve. Each curve was resolved into 1024 time channels of 9.8 ps. The light source was a diode laser of 2.5 mW average power, 785 nm wavelength, and 50 MHz repetition rate. The left sequence was detected with a source-detector distance of 8 cm, and the right sequence with a distance of 5 cm. The count rates were 1.8×10^5 s^{-1} and 4.5×10^6 s^{-1} respectively. These correspond to average numbers of 18,000 and 450,000 photons recorded per curve. The relative standard deviations of the photon numbers are 7.5×10^{-3} and 1.5×10^{-3}. The standard deviations of the first moments, m_1, are approximately 800 fs and 4 ps. These values are of the same order as the haemodynamic response of the brain to motor stimulation. Consequently, the haemodynamic response can be recorded by averaging over a moderate number of stimulation events [26,27].

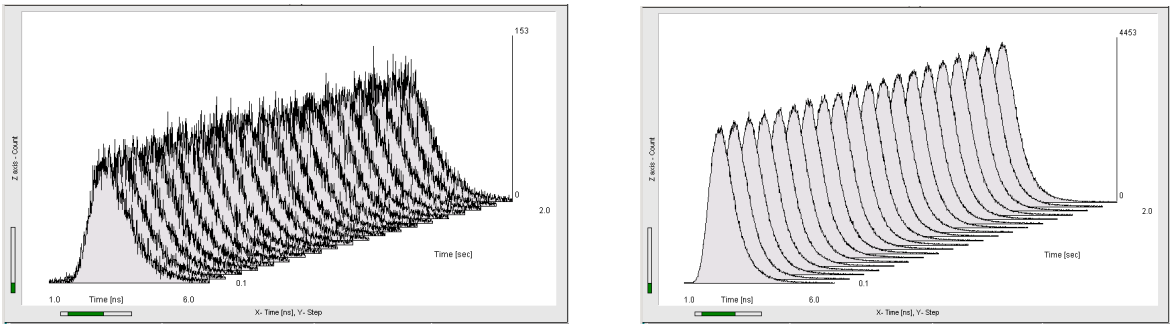

Fig. 4: 20 steps of a TOF sequence recorded at an adult human head by TCSPC memory swapping. Acquisition time 100 ms per curve, 1024 time channels per curve, time channel width 9.8 ps. Count rate $1.8 \cdot 10^5$ s^{-1} (left) and $4.5 \cdot 10^6$ s^{-1} (right)

Phantom experiment

An imaging probe for optical topography experiments was constructed, which consists of an array of eight detector fibre bundles and two source fibres mounted on a thin rectangular aluminium plate. The arrangement, shown in Fig. 5, was similar in design to the probe used by Franceschini *et al* [16] to image functional activation of the motor cortex. The lower surface of the plate was lined with a soft, light-absorbing foam, 10 mm thick, with suitable holes for the sources and detectors. To evaluate the probe, a solid epoxy resin phantom was built in the form of a slab, with dimensions 170 x 90 x 59 mm, and with uniform optical properties of $\mu_s' = 1.0$ mm^{-1} and $\mu_a = 0.01$ mm^{-1}. A hole, 10 mm in diameter, was drilled across the slab at a constant depth of 15 mm below the top surface. A cylindrical epoxy resin rod was made with

a length of 110 mm, which fits exactly within the hole. The rod has the same optical properties of the slab except for a section 10 mm in length in the middle of the rod which has optical properties of $\mu_s' = 1.0\ mm^{-1}$ and $\mu_a = 0.1\ mm^{-1}$ (i.e. ten times greater absorption). The rod may be moved within the hole, enabling the position of the high absorption section to be moved from one side of the slab to the other.

The detector fibre bundles were eight of the 32 available on the UCL time-domain imaging system, known as MONSTIR [38]. Four bundles were coupled to one 8-anode MCP-PMT and four to another. However, instead of using the usual MONSTIR TCSPC electronics, the pre-amplified outputs of the MCP-PMTs were connected to one of the TCSPC engines on an SPC card via an 8-channel router. This enables data to be recorded continuously, without the read-out time of several seconds between sources which had previously inhibited the use of MONSTIR for fast, optical topography studies of functional activation.

The probe was placed on the phantom, with the foam in contact with the top surface. The high-absorbing section of the rod was initially located at position **A**, as indicated in fig. 5. Each source (780 nm, 10 mW) was then activated for five seconds while time-of-flight data was recorded at each detector position simultaneously. The rod was then moved so that the high-absorbing section was translated to position **B**. Both sources were again activated for five seconds each while another set of data was recorded. The whole process was then repeated ten times.

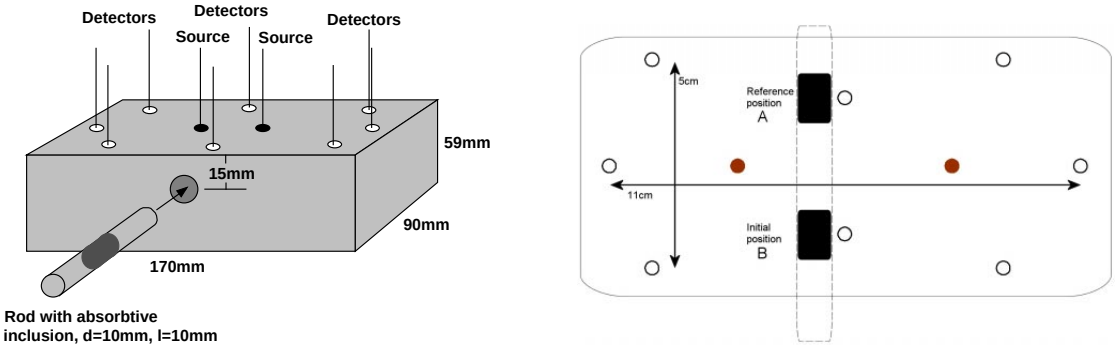

Fig. 5: A probe consisting of eight detectors (open circles) and two sources (filled circles) mounted on a solid slab phantom. A rod located 15 mm below the top surface contains a high-absorbing section which was translated to positions A and B.

Measurements of integrated intensity and mean flight time were calculated from the histograms of photon flight times recorded by each detector for each source, and averaged for the ten repeated acquisitions. Intensity ratios and differences in mean flight time generated from the two sets of data were then employed to reconstruct three-dimensional (3D) images of the slab, representing the *change* in absorption. A fast, linear algorithm was employed. The Jacobian was calculated using the finite element method [1] and inverted following Tikhonov regularisation.

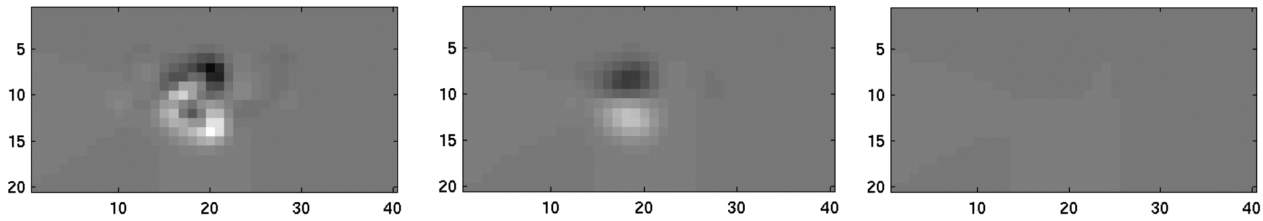

Fig. 6: Horizontal (transverse) slices across the three-dimensional image representing the change in absorption as the rod was moved from position A to position B. The slices correspond to 7.5 mm (left), 17.5 mm (middle), and 27.5 mm (right) below the top surface of the phantom. The actual depth of the rod corresponds approximately to the middle slice. Measurement and reconstruction artefacts contribute to the top slice.

A 3D image representing the change in absorption as the rod was moved from position A to position B is shown in fig. 6 as a series of three slices representing depths of 7.5 mm, 17.5 mm, and 27.5 mm below the surface. As expected, the

images reveal a localised region of increased absorption and a localised region of decreased absorption due to the translation of the high-absorbing region of the rod.

4. SUMMARY

Multi-dimensional TCSPC is a promising signal acquisition technique for diffuse optical tomography. A single TCSPC channel is able to simultaneously acquire the signals of several detectors. Moreover, several lasers and source positions can be multiplexed at high rate. Sequences of time-of-flight data can be recorded at a rate of 100 ms per curve. A single TCSPC channel can be operated at a count rates of several 10^6 photons per second. Four TCSPC channels can be operated in parallel in a single standard PC. With H5773-20 detectors, the instrument response functions remain stable within 2 ps for recorded count rates as high as 4×10^6 photons per second. The technique appears suitable for static brain imaging by a large number of detector channels and multiplexed source channels. Moreover, the fast sequential recording capability makes the technique exceptionally useful for imaging haemodynamic effects in the brain. Other potential applications are fluorescence detection in DOT, small-animal imaging, and combinations of DOT with fast optical beam scanning.

5. REFERENCES

1. S. R. Arridge, J. C. Hebden, M. Schweiger, F. E. W. Schmidt, M. E. Fry, E. M. C. Hillman, H. Dehghani, and D. T. Delpy, "A method for three-dimensional time-resolved optical tomography," *Int. J. Imag. Sys. Tech*. **11**, 2-11, 2000.
2. A. Bassi, J. Swartling, J. D'Andrea, A. Pifferi, A. Torricelli, and R. Cubeddu, "Time-resolved spectrophotometer for turbid media based on supercontinuum generation in a photonic crystal fibre," *Opt. Lett*. **29**, 2405-2507, 2004.
3. W. Becker, A. Bergmann, H. Wabnitz, D. Grosenick, and A. Liebert, "High count rate multichannel TCSPC for optical tomography," *Proc. SPIE* **4431**, 249-254, 2001.
4. W. Becker, A. Bergmann, G. Biscotti, K. Koenig, I. Riemann, L. Kelbauskas, and C. Biskup, "High-Speed FLIM Data Acquisition by Time-Correlated Single Photon Counting," *Proc. SPIE* **5323**, 27-35, 2004.
5. W. Becker, A. Bergmann, M. A. Hink, K. König, K. Benndorf, and C. Biskup, "Fluorescence lifetime imaging by time-correlated single photon counting," *Micr. Res. Techn*. **63**, 58-66, 2004.
6. W. Becker, A. Bergmann, C. Biskup, T. Zimmer, N. Klöcker, and K. Benndorf, "Multi-wavelength TCSPC lifetime imaging," *Proc. SPIE* **4620**, 79-84, 2002.
7. W. Becker, H. Hickl, C. Zander, K. H. Drexhage, M. Sauer, S. Siebert, and J. Wolfrum, "Time-resolved detection and identification of single analyte molecules in microcapillaries by time-correlated single photon counting," *Rev. Sci. Instrum*. **70**, 1835-1841, 1999.
8. Becker & Hickl GmbH (2003) SPC-134 through SPC-830 time-correlated single photon counting modules, application manual. Available on *www.becker-hickl.com* .
9. Becker & Hickl GmbH, BHP-600, BHLP-700 near-infrared picosecond diode laser modules. Available on *www.becker-hickl.com* .
10. B. Chance, M. Cope, E. Gratton, N. Ramanujam, and B. Tromberg, "Phase measurement of light absorption and scatter in human tissue," *Rev. Sci. Instrum*. **69**, 3457-3481, 1998.
11. J. Chang, H. L. Graber, and R. L. Barbour, "Imaging of fluorescence in highly scattering media," *IEEE Trans. on Biomed. Eng*. **44**, 810-822, 1997.
12. R. Cubeddu, A. Pifferi, P. Taroni, A. Torricelli, and G. Valentini, "Noninvasive absorption and scattering spectroscopy of bulk diffuse media: An application to the optical characterization of human breast," *Appl. Phys. Lett*. **74**, 874-876, 1999.
13. T. Desmettre, J. M. Devoisselle, and S. Mordon, "Fluorescence properties and metabolic features of indocyanine green (ICG) as related to angiography," *Elsevier Science: Survey of Ophthalmology*, Vol. **45**, 1-15, 2000.
14. C. Dunsby and P. M. W. French, "Techniques for depth-resolved imaging through turbid media including coherence-gated imaging," *J. Phys. D: Appl. Phys*. **36**, 207-227, 2003.
15. J. J. Farrell and M. S. Patterson, "Diffusion modeling of fluorescence in tissue," In Mycek M-A, Pogue BW (eds) Handbook of Biomedical Fluorescence. Marcel Dekker Inc. New York, Basel, pp 29-60, 2003.
16. M. A. Franceschini, V. Toronov, M. E. Filiaci, E. Gratton, and S. Fantini, "On-line optical imaging of the human brain with 160-ms temporal resolution," *Opt. Expr*. **6**, 49-57, 2000.

17. P. Gallant, A. Belenkov, G. Ma, F. Lesage, Y. Wang, D. Hall, and L. A. McIntosh, "A quantitative time-domain optical imager for small animals in vivo fluorescence studies,". In OSA Biomedical Optics Topical Meetings on CD ROM (The Optical Society of America, Washington, DC) WD2, 2004.
18. D. Grosenick, K. T. Moesta, H. Wabnitz, J. Mucke, C. Stroszcynski, R. MacDonald, P. M. Schlag, and H. Rinneberg, "Time-domain optical mammography: initial clinical results on detection and characterization of breast tumors," *Appl. Opt*. **42**(16), 3170-3186, 2003.
19. D. Grosenick, H. Wabnitz, K. T. Moesta, J. Mucke, M. Möller, C. Stroszczynski, J. Stößel, B. Wassermann, P. M. Schlag, and H. Rinneberg, "Concentration and oxygen saturation of haemoglobin of 50 breast tumours determined by time-domain optical mammography," *Phys. Med. Biol*. **49**, 1165-1181, 2004.
20. Hamamatsu Photonics K.K., H5773/H5783/H6779/H6780/H5784 Photosensor modules, 2001.
21. J. C. Hebden, F. E. W. Schmidt, M. E. Fry, M. Schweiger, E. M. C. Hillman, D. T. Delpy, and S. R. Arridge, "Simultaneous reconstruction of absorption and scattering images by multichannel measurement of purely temporal data," *Opt. Lett*. **24**, 534-536, 1999.
22. J. C. Hebden, A. Gibson, T. Austin, R. Md Yusof, N. Everdell, D. T. Delpy, S. R. Arridge, J. H. Meek, and J. S. Wyatt, "Imaging changes in blood volume and oxygenation in the newborn infant brain using three-dimensional optical tomography," *Phys. Med. Biol*. **49**, 1117-1130, 2004.
23. F. F. Jöbsis, "Noninvasive, infrared imaging of cerebral and myocardial oxygen sufficiency and circulatory parameters," *Science* **198**, 1264-1267, 1977.
24. J. R. Lakowicz, Principles of Fluorescence Spectroscopy, 2nd ed., Plenum Press, New York, 1999.
25. A. Liebert, H. Wabnitz, D. Grosenick, M. Möller, R. Macdonald, and H. Rinneberg, "Evaluation of optical properties of highly scattering media by moments of distributions of times of flight of photons," *App. Opt*. **42**, 5785-5792, 2003.
26. A. Liebert, H. Wabnitz, J. Steinbrink, H. Obrig, M. Möller, R. Macdonald, A. Villringer, and H. Rinneberg, "Time-resolved multidistance near-infrared spectroscopy at the human head: Intra- and extracerebral absorption changes from moments of distribution of times of flight of photons," *Appl. Opt*. **43**, 3037-3047, 2004.
27. A. Liebert, H. Wabnitz, J. Steinbrink, M. Möller, R. Macdonald, H. Rinneberg, A. Villringer, and H. Obrig, "Bed-side assessment of cerebral perfusion in stroke patients based on optical monitoring of the dye bolus by time-resolved diffuse reflectance," *NeuroImage* **24**, 426-435, 2005.
28. T. O. McBride, B. W. Pogue, E. D. Gerety, S. D. Poplack, U. L. Österberg, and K. D. Paulsen, "Spectroscopic diffuse optical tomography for the quantitative assessment of hemoglobin concentration and oxygen saturation in breast tissue," *Appl. Opt*. **38**, 5480, 1999.
29. T. O. McBride, B. W. Pogue, S. Jiang, U. L. Österberg, and K. D. Paulsen, "A parallel-detection frequency-domain near-infrared tomography system for hemoglobin imaging of the breast in vivo," Rev. Sci. Instrumen. **72**, 1817, 2001.
30. A. B. Milstein, J. J. Stott, S. Oh, D. A. Boas, and R. P. Millane, "Fluorescence optical tomography using multiple-frequency data," *J. Opt. Soc. Am. A* **21**, 1035-1049, 2000.
31. S. Mordon, J. M. Devoisselle, and S. Soulie-Begu, "Indocyanine green: physicochemical factors affecting its fluorescence in vivo," *Microvascular Research* **55**, 146, 1998.
32. S. P. Morgan and K. Y. Yong, "Elimination of amplitude-phase crosstalk in frequency domain near-infrared spectroscopy," *Rev. Sci. Instrumen*. **72**, 1984-1987, 2001.
33. I. Nissilä, K. Kotilahti, K. Fallström, and T. Katila, "Instrumentation for the accurate measurement of phase and amplitude in optical tomography," Rev. Sci. Instrumen. **73**, 3306, 2002.
34. V. Ntziachristos, X. H. Ma, A. G. Yodh, and B. Chance, "Multichannel photon counting instrument for spatially resolved near infrared spectroscopy," *Rev. Sci. Instrum*. **70**, 193-201, 1999.
35. V. Ntziachristos and B. Chance, "Accuracy limits in the determination of absolute optical properties using time-resolved NIR spectroscopy," *Med. Phys*. **28**, 1115-1124, 2001.
36. D. V. O'Connor and D. Phillips. Time Correlated Single Photon Counting. Academic Press, London, 1984.
37. M. D. O'Leary, D. A. Boas, X. D. Li, B. Chance, and A. G. Yodh, "Fluorescence lifetime imaging in turbid media," *Opt. Lett*. **21**, 158-160, 1996.
38. F. E. W. Schmidt, M. E. Fry, E. M. C. Hillman, J. C. Hebden, and D. T. Delpy, "A 32-channel time-resolved instrument for medical optical tomography," *Rev. Sci. Instrum*. **71**, 256-265, 2000.
39. E. M. Sevick-Muraca, A. Godavarty, J. P. Houston, A. B. Thompson, and R. Roy, "Near-infrared imaging with fluorescence contrast agents." In Mycek M-A, Pogue BW (eds) Handbook of Biomedical Fluorescence. Marcel Dekker Inc. New York, Basel, pp 445-527, 2003.

40. J. Steinbrink, H. Wabnitz, H. Obrig, A. Villringer, and H. Rinneberg, “Determining changes in NIR absorption using a layered model of the human head,” *Phys. Med. Biol*. **46**, 879-896, 2001.
41. P. Taroni, G. Danesini, A. Torricelli, A. Pifferi, L. Spinelli, and R. Cubeddu, “Clinical trial of time-resolved scanning optical mammography at 4 wavelengths between 683 and 975 nm,” *J. Biomed. Opt*. **9**, 464-473, 2004.
42. A. Torricelli, L. Spinelli, A. Pifferi, P. Taroni, and R. Cubeddu, “Use of a nonlinear perturbation approach for in vivo breast lesion characterization by multi-wavelength time-resolved optical mammography,” *Opt. Expr*. **11**, 853-867, 2003.
43. B. C. Wilson and S. L. Jacques, “Optical reflectance and transmittance of tissues: Principles and application,” IEEE *J. Quant. Electron*. **26**, 2186-2199, 1990.